Journal of Power Sources 262 (2014) 444–450

Contents lists available at ScienceDirect

Journal of Power Sources

journal homepage: www.elsevier.com/locate/jpowsour

Stable quasi-solid-state dye-sensitized solar cell using a diamide derivative as low molecular mass organogelator

Li Tao [a,1], Zhipeng Huo [a,**,1], Songyuan Dai [a,b,*], Jun Zhu [a], Changneng Zhang [a], Yang Huang [a], Bing Zhang [b], Jianxi Yao [b]

[a] Key Laboratory of Novel Thin-Film Solar Cells, Division of Solar Energy Materials and Engineering, Institute of Plasma Physics, Chinese Academy of Sciences, Hefei, Anhui 230031, PR China
[b] State Key Laboratory of Alternate Electrical Power System with Renewable Energy Sources, North China Electric Power University, Beijing 102206, PR China

HIGHLIGHTS

- A diamide derivative is used as LMOG to gelate liquid electrolyte.
- A novel and intrinsic stable gel electrolyte with high T_{gel} is prepared.
- The kinetic processes of electron transport and recombination are investigated.
- The QS-DSSC exhibits excellent stability during the accelerated aging tests.

GRAPHICAL ABSTRACT

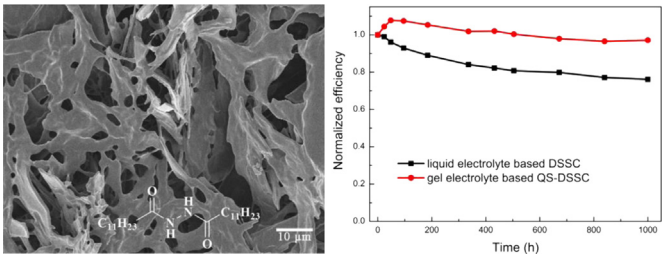

ARTICLE INFO

Article history:
Received 27 January 2014
Received in revised form
12 March 2014
Accepted 26 March 2014
Available online 12 April 2014

Keywords:
Dye-sensitized solar cell
Quasi-solid-state
Electrolyte
Low molecular mass organogelator
Electron transport and recombination
Stability

ABSTRACT

High stability is a significant target for practical applications of dye-sensitized solar cells. 2-(1-oxododecyl)hydrazide, a diamide derivative, is synthesized and applied in quasi-solid-state dye-sensitized solar cells (QS-DSSCs) as a low molecular mass organogelator (LMOG). It is noteworthy that the transition temperature from gel state to liquid state (T_{gel}) of this gel electrolyte is 125.2 °C, which ensures the gel state of the electrolyte at the DSSC operating temperature. The influences of the gel electrolyte on the kinetic processes of electron transport and recombination are investigated. The diffusion of redox species in the gel electrolyte is hindered by the crosslinked network, and the decreased electron recombination lifetime indicates an increased electron recombination in QS-DSSC. Significantly, the QS-DSSC exhibits excellent thermal and light-soaking stabilities during accelerated aging tests for 1000 h. Especially, there is almost no change in the short-circuit current density (J_{sc}) in the QS-DSSC, while the J_{sc} of the liquid electrolyte based DSSC decreases to 79–90% of their initial values. These results are very important for the application and commercialization of DSSCs.

1. Introduction

Since the original development of sensitized nanocrystalline solar cells (DSSCs) by Michael Grätzel and his coworkers [1], DSSCs are considered to be one of the emerging solar technologies that offers the potential to reduce the cost of photovoltaic electricity generation. It is clear that stability is a prerequisite for application of any photovoltaic technology and the extent of application is limited by the level of stability that can ultimately be achieved. The

* Corresponding author. Key Laboratory of Novel Thin-Film Solar Cells, Division of Solar Energy Materials and Engineering, Institute of Plasma Physics, Chinese Academy of Sciences, Hefei, Anhui 230031, PR China. Tel.: +86 10 61772268.
** Corresponding author. Tel.: +86 551 65592190.
E-mail addresses: zhipenghuo@163.com (Z. Huo), sydai@ipp.ac.cn, solar@ipp.ac.cn (S. Dai).
[1] Li Tao and Zhipeng Huo contributed equally to this work.

http://dx.doi.org/10.1016/j.jpowsour.2014.03.128
0378-7753/

electrolyte is one of the key components of DSSCs and its properties greatly affect the photovoltaic conversion efficiencies and stability of DSSCs [2,3]. And the organic solvent liquid electrolyte based DSSCs have been optimized to achieve the power conversion efficiency exceeding 12% [4], however, the volatile solvent in liquid electrolyte usually results in leakage and evaporation, which is considered as one of the critical factors limiting the long-term performance and practical use of DSSCs. Many alternatives have been made to overcome this problem by replacing the liquid electrolytes, including inorganic or organic hole conductors and polymer gel electrolytes. However, derivative problems such as contact between hole transporting materials and the nanoporous semiconductor films are remain to be solved. Therefore, the quasi-solid-state electrolyte which formed by low molecular mass organogelators (LMOGs) arouses wide concern. At proper temperature, the LMOGs can self-assemble through H-bonds, van der Waals Forces, π–π bond and lead to a three-dimensional network which immobilizes the liquid solvent. The formed gel can be melted above the transition temperature from gel state to liquid state (T_{gel}) and reformed gel below this temperature. This thermal reversible nature is beneficial to the fabrication of DSSCs. A lot of components, such as 12–hydroxystearic acid [5], cyclohexanecarboxylic acid-[4-(3-octadecylureido)phenyl]amide [6], tetradodecylammonium bromide [7] and 1,3:2,4-di-O-benzylidene-d-sorbitol derivatives [8] have been developed as LMOGs and applied in the quasi-solid-state dye-sensitized solar cells (QS-DSSCs).

In this work, we synthesize 2-(1-oxododecyl)hydrazide and used it as LMOG to gelate 3-methoxypropionitrile (MePN) based liquid electrolyte to obtain a novel gel electrolyte. The kinetic processes of electron transport and recombination, the photovoltaic performance and both the thermal and light-soaking stabilities of the corresponding QS-DSSC were investigated in detail.

2. Experimental

2.1. Electrolyte preparation

The 2-(1-oxododecyl)hydrazide compound was synthesized according the literature [9]. 1,2-Methyl-3-propylimidazoliumiodide (DMPII) was prepared as reported previously [10]. The liquid electrolyte for DSSCs was composed of 0.1 mol L^{-1} iodine (I_2: 99%, Aldrich), 0.1 mol L^{-1} anhydrous lithium iodide (LiI: 99%, Aldrich), 0.5 mol L^{-1} N-methylbenzimidazole (NMBI: 99%, Aldrich), and 1 mol L^{-1} DMPII in 3-methoxypropionitrile (MePN: 99%, Fluka). Gel electrolytes with different concentrations of gelator were prepared by adding 2-(1-oxododecyl)hydrazide into liquid electrolyte and heated under stirring until the gelator melted. The gel electrolytes were formed after cooling to room temperature. The selection of the concentration of gelator for further study in this work is described in the Supporting Information.

2.2. Fabrication of dye-sensitized solar cells

The nanocrystalline electrodes about 11.3 μm thickness were obtained by screen–printing TiO_2 paste on FTO glass (TEC-8, LOF). After sintering at 450 °C for 30 min in air then cooling to 120 °C, the nanoporous TiO_2 photoelectrodes were immersed in an ethanol solution of 0.5 mmol L^{-1} cis–dithiocyanate-*N*,*N*–bis-(4–carboxylate-4-tetrabutylammoniumcarboxylate-2,2- bipyridine) ruthenium (II) (N719 dye) for 14 h. The platinized counter electrodes were obtained by spraying H_2PtCl_6 solution to FTO glass followed by heating at 410 °C for 20 min. DSSCs were assembled by sealing the dyed nanoporous TiO_2 photoelectrode and the counter electrode with a thermal adhesive film (Surlyn 1702, Dupont, USA). The liquid electrolyte was injected into the internal space between of two electrodes through the hole on the counter electrode, which was later sealed by a cover glass and thermal adhesive film. The gel electrolyte was heated to 135 °C under stirring until the gel transform to liquid completely. Then, the electrolyte (hot solution) was rapidly injected into the cell and the cell was sealed as the same as the liquid electrolyte based DSSC. After cooling to room temperature, a uniform motionless gel layer was formed in cell.

2.3. Differential scanning calorimetry (DSC)

The transition temperature from gel state to liquid state (T_{gel}) of the gel electrolyte was determined by differential scanning calorimeter (DSC–Q2000, TA, USA). Approximately 5–7 mg of each sample was weighed and sealed in an aluminum pan and heated at a rate of 10 °C min^{-1} under nitrogen flow from 25 to 145 °C for DSC measurement.

2.4. Field emission scanning electron microscopy (FE-SEM)

Field emission scanning electron microscopy (JSM-6330F, JEOL, Japan) was used for investigating the morphology of the gel. And the xerogel sample was prepared by drying the gel (8 wt% gelator in MePN) at ambient temperature.

2.5. Linear sweep voltammetry measurements

Linear sweep voltammograms were recorded on a electrochemical workstation (Autolab 320, Metrohm, Switzerland) at 25 °C in two–electrode mode of DSSCs equipped with a 5.0 μm platinum ultramicroelectrode (CHI107, CH Instruments Inc., USA) as working electrode, a 1 mm radius platinum disk electrode (CHI102, CH Instruments Inc., USA) as counter electrode and reference electrode [19,20]. The linear sweep voltammograms were obtained at scan rate of 5 mV s^{-1}.

2.6. Electrochemical impedance spectroscopy (EIS) measurement

EIS measurement of DSSCs was recorded with an electrochemical analyzer (Autolab 320, Metrohm, Switzerland). To measure the impedance, a direct-current bias at 600 mV, and a perturbation amplitude of 10 mV within the frequency range from 10 MHz to 10 mHz was applied in dark. The obtained impedance spectra were fitted with Z-view software (v2.8b, Scribner Associates, USA) in terms of a transmission line equivalent circuit model to interpret the characteristics of DSSCs [11,12].

2.7. Controlled intensity modulated photocurrent/photovoltage spectroscopy (IMPS/IMVS) measurements

The experimental setup for IMPS and IMVS measurements have been described elsewhere [13–15]. Intensity–modulated measurements were carried out by an electrochemical workstation (IM6e, Zahner, Germany) with light emitting diodes (LED) (λ = 610 nm) driven by export (Zahner, Germany). The LED provided both the dc and ac components of the illumination. A small ac component is 10% or less than that of the dc component and the frequency range was 3 kHz–300 mHz.

2.8. Characterization of incidental photon-to-electron conversion efficiency (IPCE)

The photocurrent action spectra were recorded on a QE/IPCE measurement kit consisting of a 300 W xenon lamp (69911, Newport, USA), a 1/4 m monochromator (74125 Oriel Cornerstone 260,

Newport, USA), a dual channel power meter (2931-C, Newport, USA) and the calibrated UV silicon photodetector (71675, Newport, USA).

2.9. Photovoltaic characterizations and stability tests

The photovoltaic performance of DSSCs with the active area of 0.16 cm^2 with black mask were measured by a Keithley 2420 digital source meter (Keithley, USA), and controlled by Test point software under a 450 W xenon lamp (Orial, USA) with a filter (AM 1.5). The incident light intensity was calibrated with a standard crystalline silicon solar cell before each experiment.

Hermetically sealed cells were used for long–term stability tests. The cells were stored in the oven at 60 °C for thermal stress experiment. Furthermore, the successive one sun light soaking experiment was also carried out. DSSCs covered with a UV cutoff filter (up to 394 nm) were irradiated at open circuit under AM 1.5, (XQ3000, 100 mW cm^{-2}, Shanghai B.R. Science Instrument Co., Ltd, China) and the ambient temperature was set to 50 °C during the light soaking experiment. These DSSCs were cooled down to the room temperature for 30 min before being measured. The *J–V* measurements were carried out from short circuit to open circuit with sampling delay time ranging from 1 ms to 1 s. The measuring integration time and step source level were fixed at 50 ms and 10 mV, respectively.

3. Results and discussion

3.1. Gelation studies of the LMOG based gel electrolyte

The morphology of the gel based on 2-(1-oxododecyl)hydrazide was visualized by scanning electron microscopy. Fig. 1 exhibits the three-dimensional network of the gel, owing to the self-assembly of gelator through the non-covalent interaction of the gelator molecule.

The transition temperature from gel state to liquid state (T_{gel}), a parameter that can be used as an indicator to reflect the thermal stability of gel electrolyte, was analyzed by differential scanning calorimetry (DSC). As shown in Fig. 2, the maximum endothermic signal appeared at 125.2 °C which corresponding to the T_{gel} of the gel electrolyte. In other word, a thermally stable gel electrolyte based on MePN electrolyte using 2-(1-oxododecyl)hydrazide was successfully prepared, and the high T_{gel} ensures the gel state of the electrolyte at the device operating temperature.

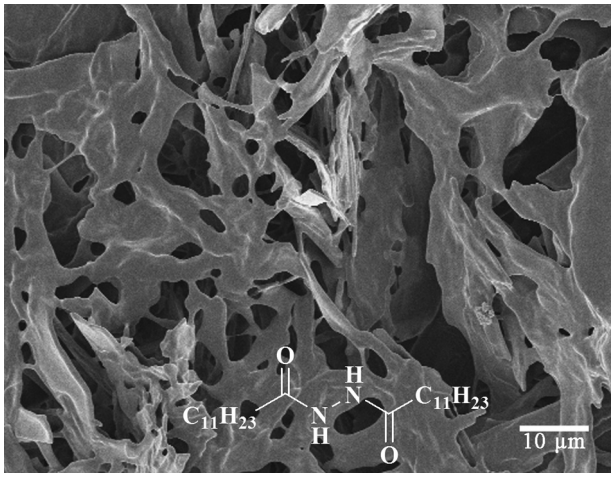

Fig. 1. SEM image of the xerogel based on 2-(1-oxododecyl)hydrazide in MePN.

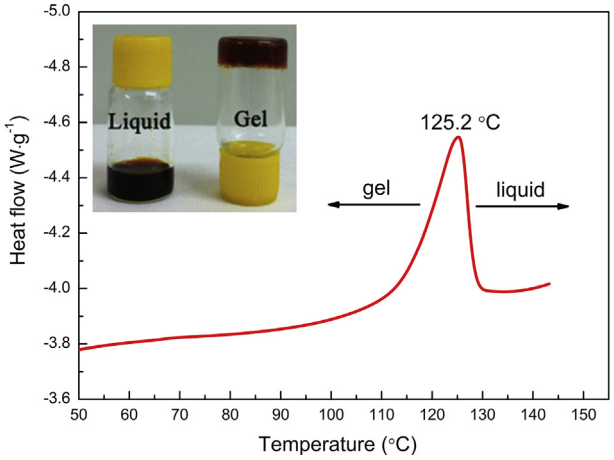

Fig. 2. Differential scanning calorimetric thermogram of LMOG based gel electrolyte.

3.2. The charge transport and electron recombination behavior

It is well documented that the diffusion rate of redox species (I^- and I_3^-) ions in electrolyte is the key factor in the DSSCs performance [16]. To understand the redox behavior of the I^- and I_3^- in the gel electrolyte, the steady-state limiting currents (i_{ss}) were determined by linear sweep voltammetry and shown in Fig. 3. The apparent diffusion coefficients (D_{app}) of I^- and I_3^- can be calculated from the following Eqn. (1) [17] and the values were listed in Table 1:

$$i_{ss} = 4nrcFD_{app} \quad (1)$$

where n is the electron number in the electrode reaction, F is the Faraday constant and c is the bulk concentration of redox species, r is the radius of the Pt ultramicroelectrode. As can be seen in Fig. 3 and Table 1, the gel electrolyte exhibits smaller D_{app} values of I^- and I_3^- than those of the liquid electrolyte, which is attributed to the hindered physical diffusion of ions caused by the crosslinked network of the gel electrolyte. The change of diffusion of I^- and I_3^- suggests that the formation of conductive pathway is altered after the liquid electrolyte being gelated by LMOG.

The kinetic processes of electron transport and recombination can be investigated by electrochemical impedance spectroscopy

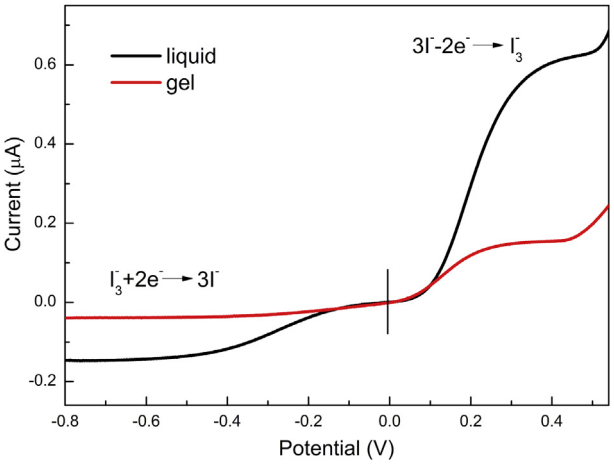

Fig. 3. Linear sweep voltammograms of liquid and gel based electrolytes with Pt ultramicroelectrode at 25 °C (scan rate = 5 mV s^{-1}).

Table 1
The steady-state limiting currents and apparent diffusion coefficients of iodide (I^-) and triiodide (I_3^-) in liquid and gel based electrolytes.

Electrolyte	$i_{ss}(I_3^-)$ (10^{-7}A)	$i_{ss}(I^-)$ (10^{-7}A)	$D_{app}(I_3^-)$ (10^{-6} cm^2 s^{-1})	$D_{app}(I^-)$ (10^{-6} cm^2 s^{-1})
liquid	1.45	6.06	3.76	4.28
gel	0.39	1.55	1.01	1.10

(EIS) [18–20]. Fig. 4 shows the chemical capacitance (C_μ), interfacial charge transfer resistance (R_{ct}) and recombination lifetime (τ_n) as a function of applied bias. Compared with the liquid electrolyte based DSSC, the C_μ for the gel electrolyte based DSSC shifts to higher potential in Fig. 4(a). This shift indicates that the TiO_2 conduction band edge shifts towards more negative potential [21–23]. It is accepted that Li^+ can interacts with the amide carbonyl groups [24]. Therefore, the adsorption of Li^+ on the surface of the mesoporous TiO_2 film was decreased by the interaction between Li^+ and the amide carbonyl groups in 2-(1-oxododecyl)hydrazide molecule in the gel electrolyte, which results in the negative shift of TiO_2 conduction band edge and leads to a decrease in excited electron injection efficiency in the gel electrolyte based DSSC [25,26].

As electrons diffuse through the mesoporous TiO_2 film by a random walk process, they may become trapped and distrapped at the surface of the TiO_2 particles and back recombine with I_3^- in electrolyte [27]. In other hand, the higher R_{ct}, which is resistance related to electron recombination processes occurring at photoelectrode/electrolyte interfaces, can lead to the slower electron recombination and the longer electron recombination time (τ_n). As is shown in Fig. 4(b) and (c), the R_{ct} and τ_n of the gel electrolyte based DSSC are lower than those of the liquid electrolyte based DSSC. This result indicates that the recombination of electron with the I_3^- in the gel electrolyte based DSSC is faster than that in the liquid electrolyte based DSSC, which is caused by the hindered I_3^- transportation from the photoelectrode/electrolyte interface to the counter electrode in the self-assembled network of the gel

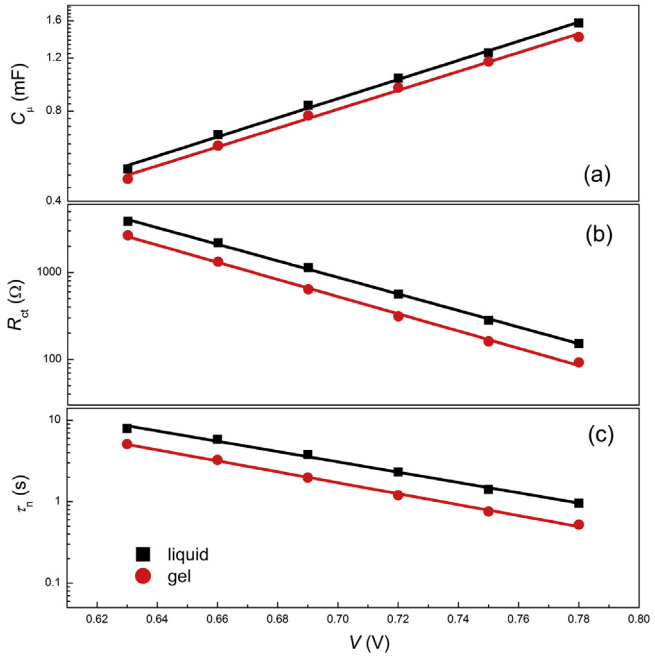

Fig. 4. Plots of (a) chemical capacitance (C_μ), (b) interfacial charge transfer resistance (R_{ct}) and (c) recombination lifetime (τ_n) as a function of applied bias.

electrolyte [26]. And the increased electron recombination is the major factor contributing to the decreased photovoltage [13].

In order to further investigate the electron transport and recombination processes of the DSSCs based on the liquid and gel electrolyte, the electron transport time (τ_{sc}) and the recombination time (τ_{oc}) were estimated from IMPS and IMVS plots, respectively. Generally, the adsorption of Li^+ on the surface of TiO_2 films can create the extra trap states and slow down the electron transportation [28]. As is shown in Fig. 5(a), the τ_{sc} of the DSSC based on the gel electrolyte was shorter than that of the DSSC based on the liquid electrolyte, which caused by the decrease absorption of Li^+ on the TiO_2 films. On the other hand, due to the faster diffusion of I_3^- and the lower recombination rate between photoinduced electrons and I_3^-, the τ_{oc} of DSSC based on the liquid electrolyte is longer than that of DSSC based on the gel electrolyte, which can be observed in Fig. 5(b).

When DSSC is working, there is a competition process between transport of the photoinduced electrons toward the external circuit and recombination of these electrons with the acceptors present in the system. The parameter of the effective electron diffusion length (L_n) and the electron collection efficiency (η_{coll}) can reflect this competition process. L_n and η_{coll} were defined as the follow equations, respectively [29,30]:

$$L_n = d\sqrt{\frac{\tau_{oc}}{2.35\tau_{sc}}} \quad (2)$$

$$\eta_{coll} = 1 - \frac{\tau_{sc}}{\tau_{oc}} \quad (3)$$

Where d is the TiO_2 layer thickness which is 11.3 μm in this work. An effective collection of charge carriers can be achieved only if the electron diffusion length is greater than the film thickness: $L_n > d$ [13,30]. Derived from the data in Fig. 5(c), the L_n values of the DSSCs based on liquid and gel electrolytes are all larger than the TiO_2 film thickness. These results ensure efficient electron collection in the TiO_2 electrode. Furthermore, the L_n and η_{coll} of the DSSC based on liquid electrolyte are higher than those of the DSSC based on gel electrolyte as shown in Fig. 5(c) and (d), which will definitely influence the incidental photon-to-electron conversion efficiency (IPCE) and photocurrent.

3.3. Photovoltaic performance and stability of QS-DSSC

The IPCE is defined as the ratio of the number of electrons in the external circuit produced by an incident photon at a given wavelength, using Eq. (4) [31,32]:

$$IPCE = \eta_{hl} \times \eta_{inj} \times \eta_{coll} \quad (4)$$

where η_{hl} is the light harvesting efficiency, η_{inj} is the excited electron injection yield and η_{coll} is the electron collection efficiency. η_{hl} is mainly determined by the amount and extinction coefficient of adsorbed dye and the light-scattering properties of the TiO_2 films, which is assumed the same in both liquid and gel electrolyte based DSSC. The location of energy level between the TiO_2 conduction band edge and excited dye largely determines the η_{inj} [25]. Therefore, the η_{inj} of the liquid electrolyte based DSSC is higher than that of the gel electrolyte based DSSC owing to the more positive TiO_2 conduction band edge potential. As can be seen in Fig. 6, the IPCE value of the DSSC based on the liquid electrolyte is higher than that of the DSSC based on the gel electrolyte due to the higher η_{inj} and η_{coll} according to the Eq. (4).

Fig. 7 shows the corresponding photocurrent density–voltage curve of the DSSCs based on the liquid and gel electrolytes at AM 1.5

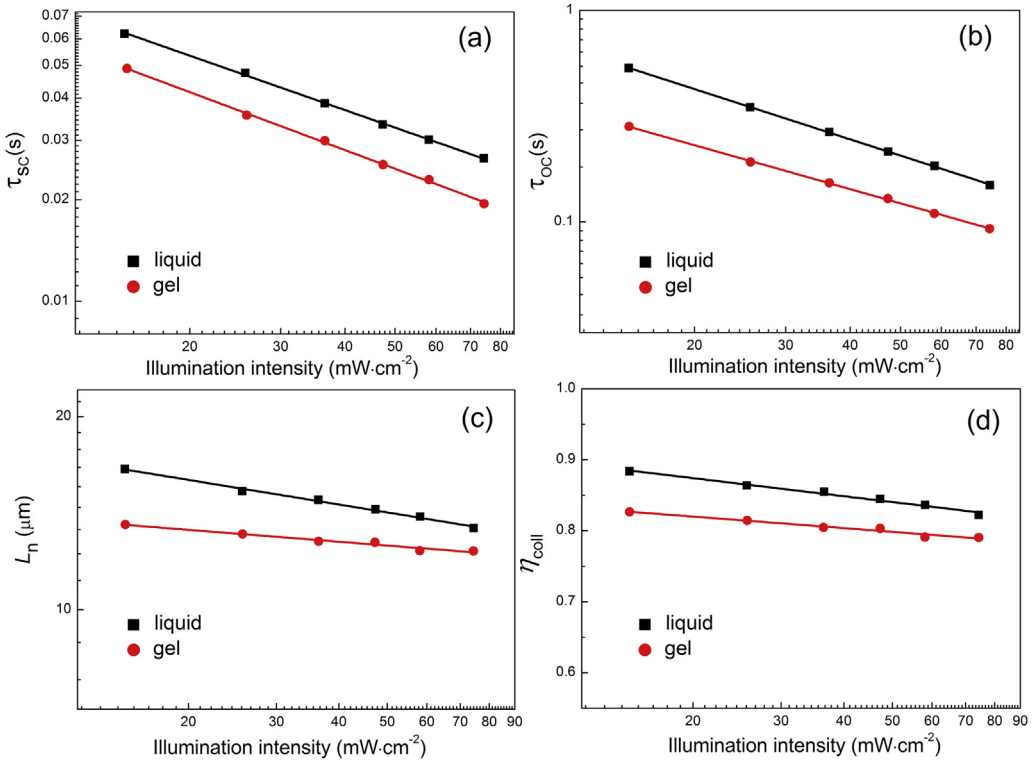

Fig. 5. (a) The light intensity dependent electron transport time (τ_{sc}), (b) the electron recombination time (τ_{oc}), (c) the effective electron diffusion length (L_n) and (d) the electron collection efficiency (η_{coll}).

and dark condition. The parameters are summarized in Table 2. The open-circuit voltages (V_{oc}), short-circuit current density (J_{sc}) and fill factors (*FF*) of the liquid electrolyte based DSSC are 714 mV, 15.87 mA cm^{-2} and 0.70, respectively, generating an photovoltaic conversion efficiencies (η) of 7.92%. The gel electrolyte does not cause noticeable variation in *FF*, but decreasing the V_{oc} and J_{sc} to 690 mV and 14.60 mA cm^{-2}, yielding a η of 7.05%. The dark current can be used to reflect the recombination between I_3^- and conduction band electrons. As can be seen in Fig. 7, the dark current of gel electrolyte based DSSC is larger than that of liquid electrolyte based DSSC, which is consistent with the changes of R_{ct} and τ_{oc}. In terms of gel electrolyte based DSSC, the TiO_2 conduction band edge shifts the negative potential which could contribute to enhance the V_{oc}, however, the gelation leads to the fast electron recombination, as a result, the V_{oc} is decreased in the gel electrolyte based DSSC as shown in Fig. 7.

Generally, J_{sc} can be approximated by the following equation [33,34]:

$$J_{sc} = q \times \mathrm{IPCE} \times I_0 \quad (5)$$

where the q is the elementary charge, I_0 is the light intensity. It is evident that the decreased J_{sc} of the gel electrolyte based DSSC is result from the lower IPCE in compared with the liquid electrolyte based DSSC.

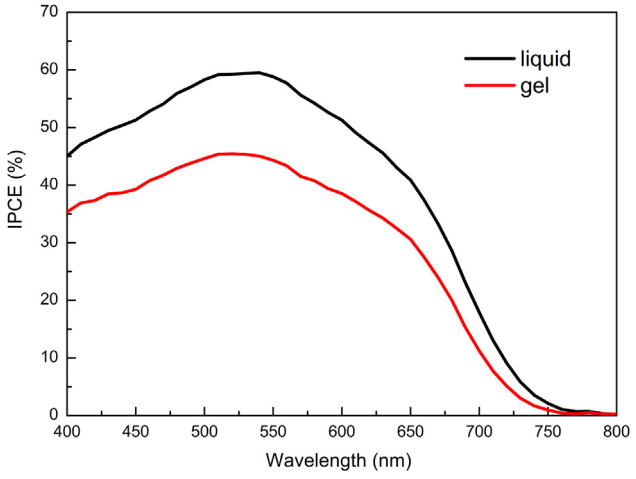

Fig. 6. IPCE spectra of DSSCs based on the liquid and gel electrolytes.

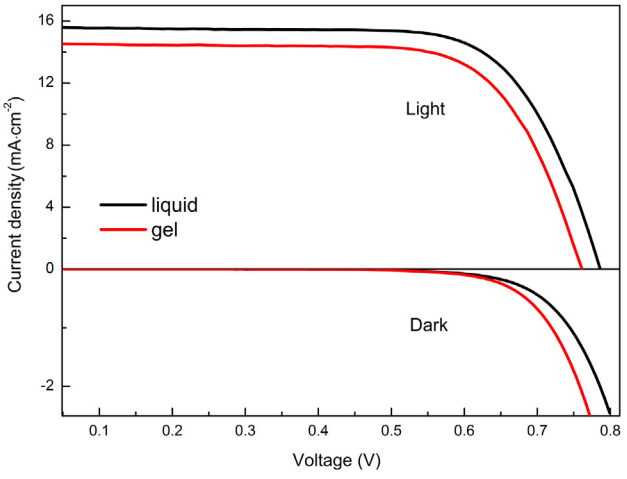

Fig. 7. *J–V* curves of the DSSCs based on liquid electrolyte and gel electrolyte under simulated AM 1.5 (the active area with a mask is 0.16 cm^2) and in the dark condition.

Table 2
The photovoltaic characteristics of DSSCs based on liquid and gel electrolytes at AM 1.5.

Cell	V_{oc} (mV)	J_{sc} (mA cm^{-2})	*FF*	η (%)
liquid	714	15.87	0.70	7.92
gel	690	14.60	0.70	7.05

Long-term stability test of this QS-DSSC is critical to access the potential for large-scale application. As shown in Fig. 8(a), the liquid electrolyte based DSSC just kept 76% of its initial value during the accelerated aging test at 60 °C for 1000 h. By contrast, the QS-DSSC based on the gel electrolyte exhibited much better stability than that of the liquid electrolyte based DSSC, which kept 97% of its initial efficiency at 60 °C for 1000 h. With nearly constant *FF* and little decrease of V_{oc}, the degradation of liquid electrolyte based device mainly results from the reduction of J_{sc}. Significantly, there is little change in the J_{sc} of gel electrolyte based DSSC, while the J_{sc} of the liquid electrolyte based DSSC decreased to 79% of its initial value. Moreover, the gel electrolyte based DSSC showed excellent light-soaking stability when the devise was subjected to the accelerated one sun light soaking experiment at 50 °C for 1000 h (covered with an UV cutoff filter). During light soaking process, there is almost no degradation in the efficiency of the gel electrolyte based DSSC (Fig. 8(b)), while the efficiency of the liquid electrolyte based DSSC decreased to 89% of its initial value. These results confirm that this gel electrolyte with high T_{gel} (125.2 °C) greatly contributes to the stability of the device by retarding evaporation and leakage of the organic solvent in the electrolyte.

4. Conclusions

In summary, 2-(1-oxododecyl)hydrazide was synthesized and successfully used as a low molecular mass organogelator to form the gel electrolyte for application in QS-DSSCs. Compared with the liquid electrolyte, the EIS and IMPS/IMVS analysis reveal that the gel electrolyte can lead to a faster interfacial charge recombination of injected electrons with I_3^- and cause a decreased open-circuit photovoltage. On the other hand, the gel electrolyte results in the relatively lower diffusion of I_3^- and I^-, excited electron injection yield and electron collection efficiency, which leads to the decreased short-circuit current density of the gel electrolyte based DSSC. Although the photovoltaic conversion efficiency is slightly lower than the corresponding liquid electrolyte based DSSC, it is very impressive that the QS-DSSC exhibits excellent thermal and light soaking stabilities during accelerated aging tests, which is

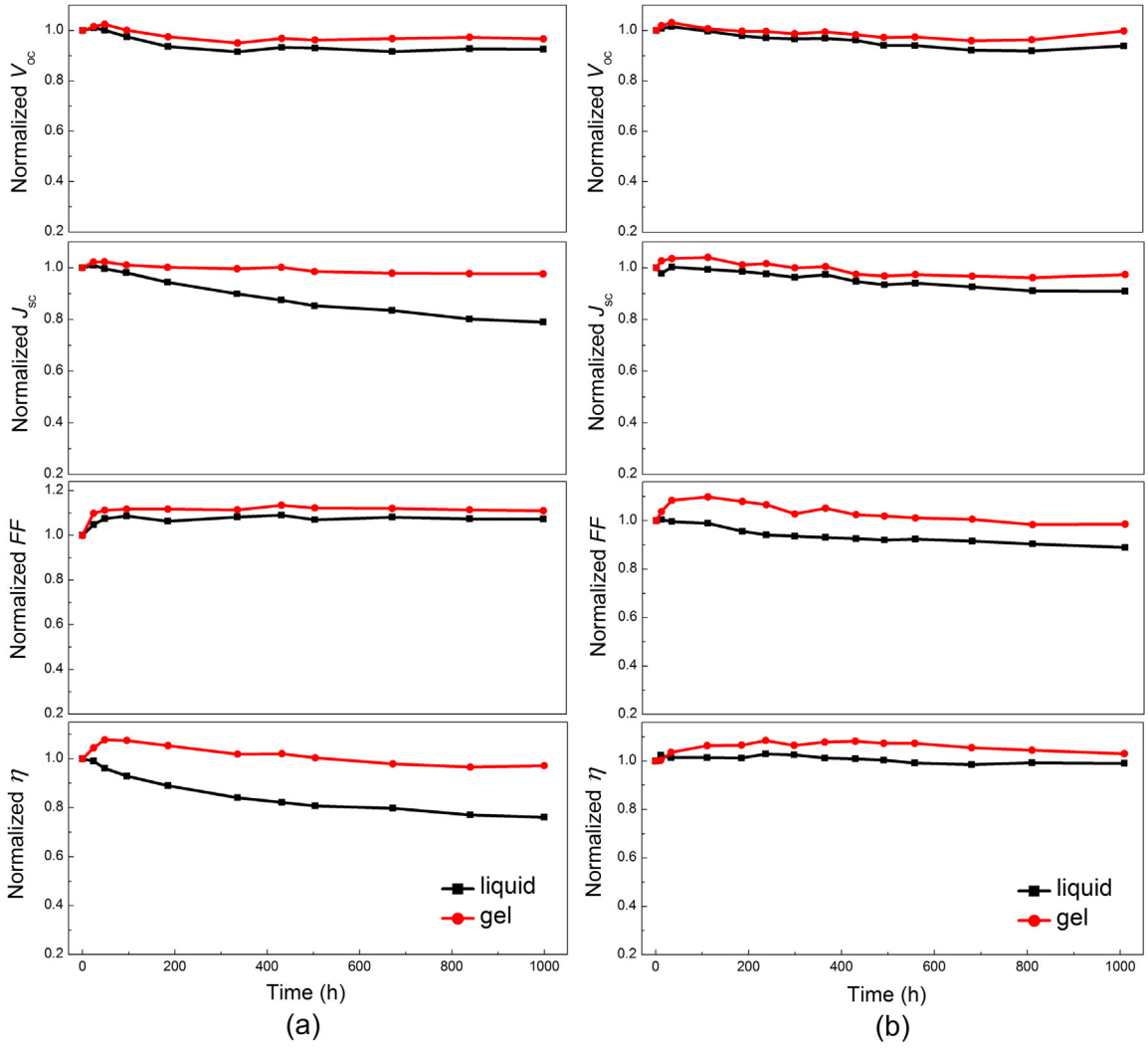

Fig. 8. Normalized efficiency variation of the DSSCs based on liquid and gel electrolytes at (a) 60 °C for 1000 h and (b) successive one sun light soaking with UV cutoff filter at 50 °C for 1000 h.

caused by the good intrinsic stability and the high T_{gel} (125.2 °C) of the gel electrolyte. And these results are very important for the application and commercialization of DSSCs.

Acknowledgments

This work was supported by the National Basic Research Program of China (No. 2011CBA00700), the National High Technology Research and Development Program of China (No. 2011AA050510), the National Natural Science Foundation of China (No. 21103197, 21173227 and 61204075) and the Program of Hefei Center for Physical Science and Technology (No. 2012FXZY006).

Appendix A. Supplementary data

Supplementary data related to this article can be found at http://dx.doi.org/10.1016/j.jpowsour.2014.03.128.

References

[1] B. Oregan, M. Grätzel, Nature 353 (1991) 737–740.
[2] M.K. Wang, C. Grätzel, S.M. Zakeeruddin, M. Gratzel, Energy Environ. Sci. 5 (2012) 9394–9405.
[3] Z. Yu, N. Vlachopoulos, M. Gorlov, L. Kloo, Dalt. Trans. 40 (2011) 10289–10303.
[4] A. Yella, H.W. Lee, H.N. Tsao, C.Y. Yi, A.K. Chandiran, M.K. Nazeeruddin, E.W.G. Diau, C.Y. Yeh, S.M. Zakeeruddin, M. Gratzel, Science 334 (2011) 629–634.
[5] Z.P. Huo, S.Y. Dai, C.G. Zhang, F.T. Kong, X.Q. Fang, L. Guo, W.Q. Liu, L.H. Hu, X. Pan, K.J. Wang, J. Phys. Chem. B 112 (2008) 12927–12933.
[6] Q.J. Yu, C.L. Yu, F.Y. Guo, J.Z. Wang, S.J. Jiao, S.Y. Gao, H.T. Li, L.C. Zhao, Energy Environ. Sci. 5 (2012) 6151–6155.
[7] Z.P. Huo, C.N. Zhang, X.Q. Fang, M.L. Cai, S.Y. Dai, K.J. Wang, J. Power Sources 195 (2010) 4384–4390.
[8] N. Mohmeyer, P. Wang, H.-W. Schmidt, S.M. Zakeeruddin, M. Grätzel, J. Mater. Chem. 14 (2004) 1905.
[9] K. Tomioka, T. Sumiyoshi, S. Narui, Y. Nagaoka, A. Iida, Y. Miwa, T. Taga, M. Nakano, T. Handa, J. Am. Chem. Soc. 123 (2001) 11817–11818.
[10] C.W. Shi, S.Y. Dai, K.J. Wang, L. Guo, X. Pan, F.T. Kong, L.H. Hu, Acta Phys. Chim. Sin. 21 (2005) 534–538.
[11] J. Bisquert, J. Phys. Chem. B 106 (2002) 325–333.
[12] M. Adachi, M. Sakamoto, J. Jiu, Y. Ogata, S. Isoda, J. Phys. Chem. B 110 (2006) 13872–13880.
[13] L.M. Peter, K.G.U. Wijayantha, Electrochim. Acta 45 (2000) 4543–4551.
[14] A.C. Fisher, L.M. Peter, E.A. Ponomarev, A.B. Walker, K.G.U. Wijayantha, J. Phys. Chem. B 104 (2000) 949–958.
[15] L. Dloczik, O. Ileperuma, I. Lauermann, L.M. Peter, E.A. Ponomarev, G. Redmond, N.J. Shaw, I. Uhlendorf, J. Phys. Chem. B 101 (1997) 10281–10289.
[16] T. Asano, T. Kubo, Y. Nishikitani, J. Photochem. Photobiol. A Chem. 164 (2004) 111–115.
[17] P. Wang, S.M. Zakeeruddin, P. Comte, I. Exnar, M. Gratzel, J. Am. Chem. Soc. 125 (2003) 1166–1167.
[18] J. Bisquert, F. Fabregat-Santiago, I. Mora-Sero, G. Garcia-Belmonte, S. Gimenez, J. Phys. Chem. C 113 (2009) 17278–17290.
[19] Q. Wang, S. Ito, M. Graetzel, F. Fabregat-Santiago, I. Mora-Sero, J. Bisquert, T. Bessho, H. Imai, J. Phys. Chem. B 110 (2006) 25210–25221.
[20] K. Park, J. Xi, Q. Zhang, G. Cao, J. Phys. Chem. C 115 (2011) 20992–20999.
[21] F. Fabregat-Santiago, G. Garcia-Belmonte, I. Mora-Sero, J. Bisquert, Phys. Chem. Chem. Phys. 13 (2011) 9083–9118.
[22] F. Fabregat-Santiago, I. Mora-Sero, G. Garcia-Belmonte, J. Bisquert, J. Phys. Chem. B 107 (2003) 758–768.
[23] E. Guillen, L.M. Peter, J.A. Anta, J. Phys. Chem. C 115 (2011) 22622–22632.
[24] J.H. Liu, X.L. Xia, Y. Li, H.J. Wang, Z.Y. Li, Struct. Chem. 24 (2013) 251–261.
[25] S.E. Koops, B.C. O'Regan, P.R.F. Barnes, J.R. Durrant, J. Am. Chem. Soc. 131 (2009) 4808–4818.
[26] N. Kopidakis, N.R. Neale, A.J. Frank, J. Phys. Chem. B 110 (2006) 12485–12489.
[27] J. Nelson, R.E. Chandler, Coord. Chem. Rev. 248 (2004) 1181–1194.
[28] D. Kou, W. Liu, L. Hu, S. Dai, Electrochim. Acta 100 (2013) 197–202.
[29] T. Oekermann, D. Zhang, T. Yoshida, H. Minoura, J. Phys. Chem. B 108 (2004) 2227–2235.
[30] M. Gratzel, Inorg. Chem. 44 (2005) 6841–6851.
[31] J.R. Mann, M.K. Gannon, T.C. Fitzgibbons, M.R. Detty, D.F. Watson, J. Phys. Chem. C 112 (2008) 13057–13061.
[32] B. Liu, W.Q. Li, B. Wang, X.Y. Li, Q.B. Liu, Y. Naruta, W.H. Zhu, J. Power Sources 234 (2013) 139–146.
[33] K. Zhu, N.R. Neale, A. Miedaner, A.J. Frank, Nano Lett. 7 (2007) 69–74.
[34] Y. Tachibana, K. Hara, K. Sayama, H. Arakawa, Chem. Mater. 14 (2002) 2527–2535.